When Two Wrongs Make a Right: Combining Aliased Arrays to Find Sound Sources

Kathleen E. Wage

Address:
Electrical and Computer Engineering (ECE) Department
George Mason University
4400 University Drive
Fairfax, Virginia 22030
USA

Email:
k.e.wage@ieee.org

Sparse array processing enables detection and localization of acoustic sources with fewer sensors than a more expensive uniform array.

Introduction

Many applications require detection and localization of sound sources. For example, sonar operators seek to detect quiet submarines in the presence of loud surface ships. Biologists aim to track vocalizing animals such as whales and birds for population surveys. Video conference designers need to automatically track speakers with the camera. A common way to detect and localize sources for applications like these is to use an array of microphones (hydrophones for underwater environments). Although a single omnidirectional microphone cannot identify the propagation direction of the sound it receives, a collection of microphones can be used to estimate the direction.

To see how localization with an array works, consider **Figure 1a** that depicts the arrival of an acoustic wave at a set of sensors located on a line (the vertical axis denoted by z). The plot assumes that the sound source is far away and that the vertical aperture spanned by the sensors is small compared with the range. Thus, the wave fronts are planar rather than spherical. The parallel lines representing the wave are separated by the wavelength λ, which is the distance between wave crests. In this model, the signal received at any point on the line is delayed or advanced

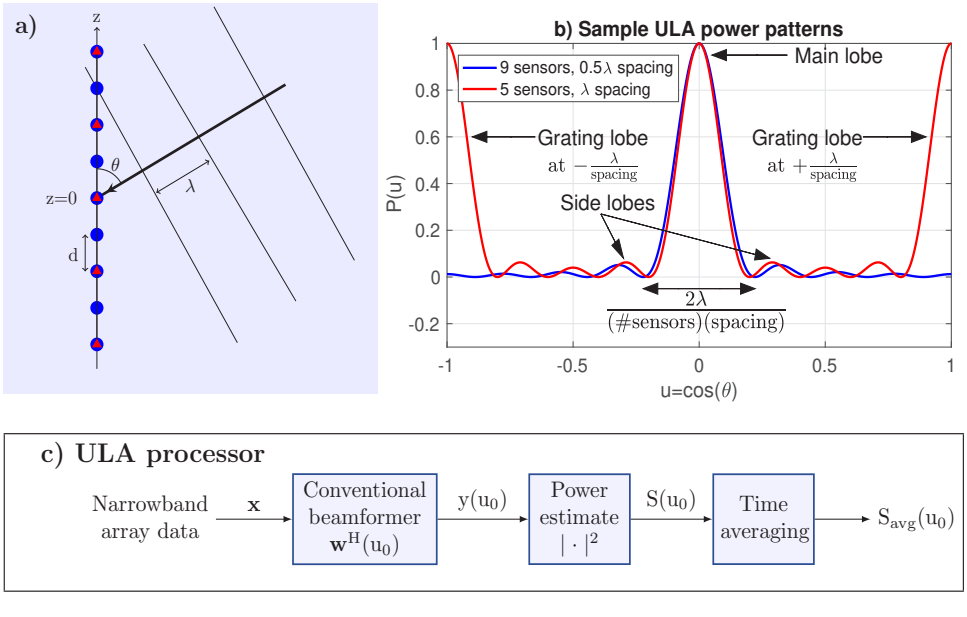

***Figure 1. a**: Planewave arriving at two linear arrays: a 9-sensor array (**blue circles**) with* d *spacing and a 5-sensor array with* 2d *spacing (**red circles**). **b**: Power patterns [P(*u*)] for these arrays, assuming* d = λ /2. ***c**: Block diagram showing how to estimate the power* S *arriving from direction* u_0 *using narrowband uniform line array (ULA) data. See text for discussion.*

from the signal received at the origin ($z = 0$). The time shift is a function of the arrival angle θ; therefore, measuring the shift allows estimation of the propagation direction. For a planewave propagating in the geometry shown in **Figure 1a**, the time shift for a sensor at z is equal to $z\cos(\theta)/c$, where c is the sound speed. When the signal arrives broadside to the array ($\theta = 90°$), it hits all the sensors simultaneously and the time shift is zero. When the signal arrives from one of the endfire directions ($\theta = 0°$ or $\theta = 180°$), the time shift is $\pm z/c$, which is the maximum value for any angle.

Suppose that the goal is to design a linear array to estimate planewave arrival angles. Two questions arise: (1) How far apart should the sensors be placed? and (2) How many sensors are required? To answer the first question, note that the time shift scales with the sensor distance. If the goal is to resolve planewaves propagating at similar angles, then it makes sense to maximize the difference in the time shifts associated with the signals. This is accomplished by placing the sensors as far apart as possible. Unfortunately, there is another consideration that limits the recommended distance between sensors. To use time shifts to identify the planewave angle, the processor must ensure that it compares the shifts between arrival times for a single wave front, which is not guaranteed when the sensor distance is too large. For instance, consider a planewave propagating down the array ($\theta = 0°$). If the sensors are separated by one wavelength (λ), the crest of one wave hits the sensor at $z = 0$ at the same time that the crest of the next wave hits the sensor at $z = \lambda$. In this case, the observed time shift will be zero, which is the same as the time shift for a broadside signal. This is an example of spatial aliasing, which occurs when a planewave propagating at one angle cannot be distinguished from a planewave propagating at a different angle based on the time delay between sensors. To guarantee unique identification of angles based on time shifts, the spatial sampling theorem says the sensors must be located less than a half-wavelength apart (Johnson and Dudgeon, 1993).

To answer the second question about the required number of sensors, consider both resolution and spatial aliasing. Angular resolution is a function of the total aperture spanned by the sensors: the larger the aperture, the better the resolution. To avoid aliasing, the sensors must be less than or equal to a half-wavelength apart. For a uniform line array (ULA), the required resolution determines the aperture and the sampling theorem determines how many sensors are required to span that aperture assuming that the sensors are equally (i.e., uniformly) spaced.

Sparse Array Processing

Sensors are expensive, and it is not always feasible to follow the design rules outlined above. Accordingly, the goal of sparse array processing is to achieve a specified angular resolution using fewer sensors than the sampling theorem requires. Sparse arrays typically use nonuniform sensor spacing. Johnson and Dudgeon (1993) and Van Trees (2002) provide useful introductions to the topic of nonuniform arrays, including summaries of the relevant literature.

This article focuses on a special class of sparse arrays and processing techniques for linear apertures, where the nonuniform sampling is implemented by interleaving two ULAs. To achieve a sparse design, one or both of the ULAs is undersampled (has sensor spacing greater than a half-wavelength).

Data processing for this type of sparse array typically consists of two stages. In the first stage, the data for each ULA is processed separately using a conventional beamformer, which is a linear filter. The second stage combines the beamformer outputs via a nonlinear operation to obtain an estimate of the spatial power spectrum (power as a function of angle). The two-stage implementation has several key advantages: (1) conventional beamforming is well understood, thus it is straightforward to design a beamformer to achieve specific performance metrics; and (2) conventional beamforming for ULAs can exploit the fast Fourier transform for computational efficiency. Assuming the interleaved ULAs are designed appropriately, the nonlinear operation eliminates aliasing introduced by undersampling. This approach to sparse array design and processing originated in seminal acoustics research by Berman and Clay (1957). The remainder of this article introduces key concepts, illustrates them using simulations, and provides references for further reading.

Conventional Uniform Line Array Processing

To lay the foundation for the discussion of sparse array processing, this section briefly reviews standard ULA processing. See the books by Johnson and Dudgeon (1993) and Van Trees (2002) for more details. The block diagram in **Figure 1c** shows how to process ULA data to estimate the power arriving at each angle. The first step is conventional beamforming. A beamformer combines the received sensor data so that the signal arriving from a desired direction adds constructively and the signals from all other directions add destructively. Assuming the desired signal is a planewave, the

conventional beamformer shifts the data for each sensor to time align the wave fronts arriving from the desired direction and then sums the time-shifted signals.

The remainder of the discussion focuses on narrowband planewave signals with temporal frequency f and wavelength $\lambda = c/f$. For a narrowband signal, beamforming reduces to applying the appropriate phase shift to the sensor data and summing. In **Figure 1c**, the input to the conventional beamformer is a complex vector x containing narrowband data from the sensors. The narrowband data is typically obtained by Fourier transforming a segment of time data for each sensor and selecting the desired frequency sample. The beamformer computes a weighted sum of the input data using the weights stored in the vector w. The complex weights are designed to implement the phase shifts required to align a planewave with arrival angle θ_0. Recall from the introduction that the phase shift is a function of the cosine of the arrival angle. Thus, the weight vector is specified in terms of directional cosine $u_0 = \cos(\theta_0)$, which defines the planewave it is designed to detect. In **Figure 1c**, the output of the conventional beamformer is $y(u_0)$, which is an estimate of the narrowband signal propagating with directional cosine u_0. The ULA processor computes an estimate of the power in the signal by squaring the beamformer output and averaging the result over time. To obtain the spatial power spectrum $S_{avg}(u_0)$, the ULA processor implements the same calculation for all possible directional cosines ($-1 \le u_0 \le +1$).

The beampattern characterizes the performance of the beamformer. The beampattern $B(u)$ is defined as the output of the beamformer when the input is a unit-amplitude planewave with directional cosine u. Essentially, the beampattern is the frequency response of the spatial filter. Because the ULA processor computes power, its performance is characterized by the power pattern $P(u)$, defined as $|B(u)|^2$. **Figure 1b** compares the power patterns for the two ULAs shown in **Figure 1a**. The first ULA has nine sensors (**Figure 1a, *blue circles***) with half-wavelength spacing ($d = \lambda/2$). The weight vector is designed for the planewave arriving broadside to the ULA [$u_0 = \cos(90°) = 0$]. The power pattern for this ULA (**Figure 1b, *blue curve***) has a peak equal to 1 at $u = u_0$, meaning that it passes the desired signal with unity gain. The main lobe defines the passband of the spatial filter and its width is inversely proportional to the ULA aperture (as quantified by the number of sensors and the sensor spacing). The sidelobes determine the filter's ability to suppress signals away from the look direction and their height is determined by the relative weighting of the sensor data (**Figure 1b** uses uniform weighting). The power pattern characterizes the performance of an array processor in resolving closely spaced sources of comparable power (main lobe width) and in detecting weak sources that may be masked by stronger sources (sidelobe height).

Now consider the power pattern (**Figure 1b, *red curve***) for the five-sensor array (**Figure 1b, *red triangles***), which spans the same aperture as the nine-sensor array using double the sensor spacing. The main lobe width for the five-sensor ULA is approximately equal to that of the nine-sensor ULA, which is expected because they span the same aperture. The primary difference between the power patterns is that the five-sensor ULA pattern includes two additional peaks away from the desired angle. These peaks are called grating lobes and they are located at multiples of $\lambda/(\text{sensor spacing})$ away from the look direction u_0. The five-sensor ULA has λ spacing, so its grating lobes are located ± 1 away from u_0 ($u_0 = 0$ in this example). This array cannot distinguish a planewave arriving at broadside ($u = 0$, $\theta = 90°$) from a planewave propagating down the array ($u = \pm 1$, $\theta = 0, 180°$). Grating lobes are a symptom of spatial aliasing, and they occur when the sensor spacing is greater than or equal to a half-wavelength.

Interleaved Sparse Arrays: Established Methods and Recent Innovations

In their seminal paper, Berman and Clay (1957) showed that it is possible to use fewer sensors to obtain the same resolution as a densely sampled ULA. They recognized that the beampattern of a large-aperture ULA can be synthesized by multiplying two smaller arrays. Berman and Clay were motivated by ideas initially proposed and implemented in radio astronomy, such as the work of Ryle (1952). Although early experiments in sonar (Welsby, 1961) and radar (Shaw and Davies, 1964) implemented product processing with densely sampled ULAs, Davies and Ward (1980) proposed interleaving a short densely sampled inner ULA with a long undersampled outer ULA and using multiplicative processing to mitigate aliasing of narrowband signals. This configuration is called a nested array and it is often used for broadband analysis because it accommodates the change in wavelength with frequency. After Pal and Vaidyanathan (2010) exploring nested arrays, Vaidyanathan and Pal (2011) proposed coprime arrays, which interleave an M-sensor ULA with an N-sensor ULA, where M and N are coprime integers (their greatest common divisor is 1). The M-sensor array has Nd spacing and the N-sensor array has Md spacing. Because d is typically $\lambda/2$, both subarrays are undersampled. Product processing can eliminate the ambiguity due to aliasing be-

cause the grating lobes of the subarrays do not overlap when M and N are coprime.

Since the early work of Berman and Clay (1957), many researchers have explored using multiplicative processing to mitigate aliasing in interleaved sparse arrays. Although this approach has been effective in many applications, it has some disadvantages. One downside of multiplicative processing is that it is not guaranteed to produce positive definite power spectral estimates (Adhikari and Buck, 2017). Another disadvantage of multiplicative processing is that it requires time averaging to reduce the impact of cross terms. As described by Pedinoff and Ksienski (1962), cross terms arise when the inputs to the subarrays contain more than one signal. When the arriving signals are uncorrelated, averaging the multiplicative processor output reduces cross-term interference. Unfortunately, there are some applications where limited data are available for averaging due to source motion or other environmental variability. Recently, both Di Martino and Iodice (2015) and Liu and Buck (2015) proposed an alternative algorithm that computes the minimum of the subarray outputs instead of multiplying them. Compared with the multiplicative processor for the same geometry, the min processor better suppresses interference away from the look direction due to its lower sidelobe levels (Liu and Buck, 2018). As discussed in **Coprime Processing**, the min processor also reduces one type of cross-term interference without requiring time averaging.

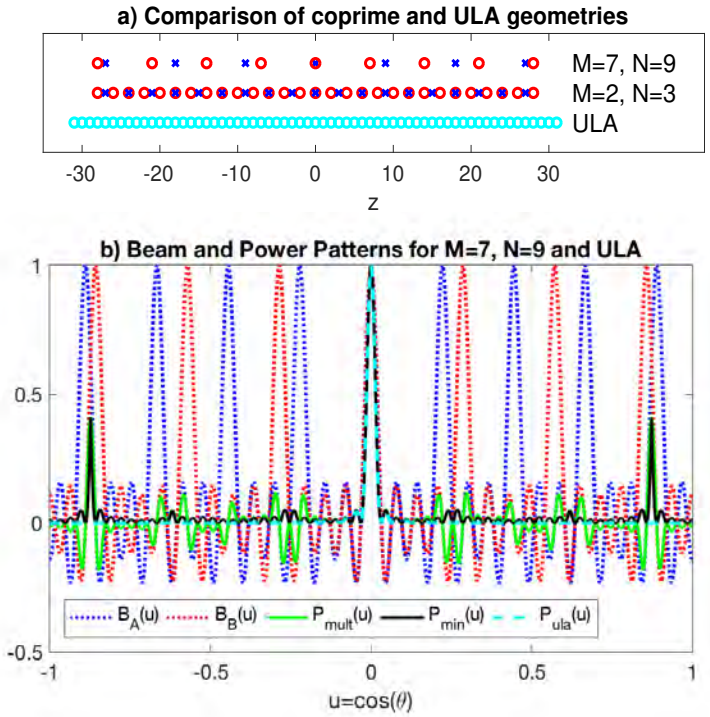

***Figure 2. a**: Sensor locations for a 7, 9 unextended coprime array (**blue crosses**), a 2, 3 extended coprime array (**red circles**), and 63-sensor ULA. All arrays assume an underlying sensor spacing of* d *= 1, which is equal to a half-wavelength for the examples. **b**: Comparison of power patterns for the ULA processor and the multiplicative and min processors for the 7, 9 coprime array. Beampatterns for the two subarrays are also shown. All patterns assume uniform weighting of the sensors normalized to guarantee unity gain in the look direction.*

Coprime Processing

This section illustrates the basic operation of multiplicative and min processors using the example of a coprime array. **Figure 2a** shows the sensor layout for an array designed with coprime factors $M = 7$ and $N = 9$. Subarray A (**Figure 2a, *blue crosses***) has seven sensors with $9d$ spacing and subarray B (**Figure 2a, *red circles)*** has nine sensors with $7d$ spacing. The subarrays share the center sensor. As shown, the coprime subarrays are symmetrical about the origin. This is a convenient assumption because it guarantees that the beampatterns are real when the arrays are steered to broadside, but it is not a requirement. For this example $d = \lambda/2$, which is set equal to 1.

Figure 3 shows the block diagrams for the multiplicative and min processors. Both processors implement conventional beamforming of the narrowband subarray data as the first step. The multiplicative processor computes the power at each angle (specified by u_0) by multiplying the outputs of the subarray beamformers (conjugating one of them), averaging the result over time, and taking the absolute value. The min processor computes the power at each angle as the minimum of the subarray power estimates and averages the result over time.

To see how these nonlinear processors eliminate the aliasing introduced by undersampling, consider the subarray beampatterns. **Figure 2b** shows the beampatterns for subarrays A and B of the 7, 9 coprime array. The main lobes of both beampatterns are located at $u = 0$ because the subarrays are steered to broadside. For broadside steering, the grating lobes of subarray A occur at multiples of $\lambda/Nd = 2/9$ and the grating lobes of subarray B occur at multiples of $\lambda/Md = 2/7$. Because M, N are coprime integers, the subarray grating lobe peaks never align. Recall that the power pattern characterizes the response of a processor to a single planewave input. The power pattern for the multiplicative processor is the product of the subarray beampatterns: $P_{mult}(u) = B_A(u) B_B^*(u)$, where $*$ indicates a complex conjugate. The power

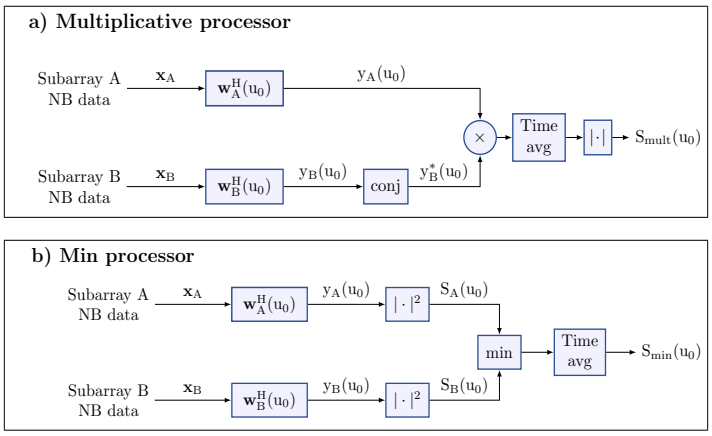

Figure 3. *Block diagrams for the multiplicative (**a**) and min (**b**) processors. Input to both processors is narrowband for each subarray. Output of each processor is an estimate of the power propagating with directional cosine* u_0. *The multiplicative processor includes an absolute value after time averaging to guarantee that* $S_{mult}(u_0)$ *is positive for plotting purposes. See text for discussion.*

pattern of the min processor is the minimum of the subarray power patterns: $P_{min}(u) = \min[|B_A(u)|^2, |B_B(u)|^2]$.

Figure 2b compares the multiplicative and min power patterns for the 7, 9 coprime array to the power pattern of a 63-sensor ULA. The plot reveals several key points about coprime array processing. First, the main lobe of the multiplicative and min processors for coprime factors *M* and *N* has the same width as the ULA processor for an *MN*-sensor ULA. Second, there are no grating lobes in $P_{mult}(u)$ and $P_{min}(u)$ because the product and min operations on the subarray beampatterns eliminate them. Third, the sidelobes of the multiplicative and min processors are higher than for the ULA processor with the same resolution. Finally, although the min power pattern is guaranteed to be positive, this is not true for the multiplicative pattern. The presence of negative sidelobes in the $P_{mult}(u)$ is the reason the multiplicative power estimate is not positive definite; see Adhikari and Buck (2017) for a discussion of this important but subtle issue.

Trading Sparsity for Sidelobe Control

Figure 2b shows that a coprime array with $M + N - 1 = 15$ sensors has the same main lobe width as a ULA with $MN = 63$ sensors. Although the coprime array requires fewer sensors, the cost of sparsity is a significant increase in sidelobes. Applications requiring lower sidelobes must sacrifice some sparsity. Adhikari et al. (2014) show that extending the coprime array by periodically repeating each subarray

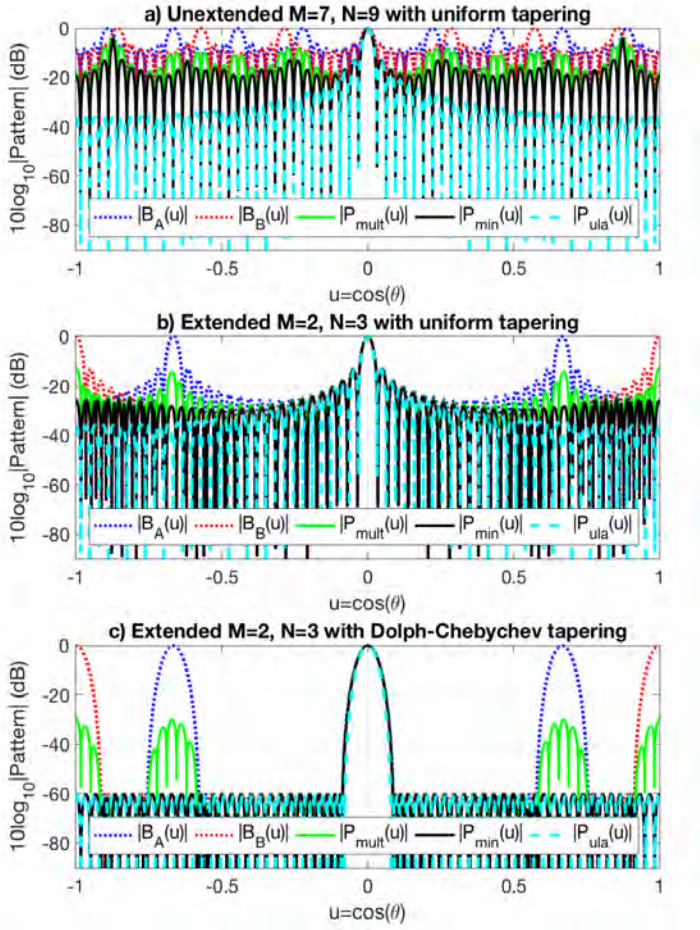

Figure 4. *Comparison of beam and power patterns for three configurations: uniformly weighted* M = *7,* N = *9 unextended coprime array (**a**), uniformly weighted* M = *2,* N = *3 coprime array extended to match the aperture of the 7, 9 coprime array (**b**), and Dolph-Chebychev-weighted extended 2, 3 coprime array (**c**). Each plot shows the patterns on a log scale; absolute value is used to avoid problems with negative sidelobes in the multiplicative pattern. The 63-sensor ULA pattern is included on each plot.*

lowers the sidelobes. Adding sensors increases the aperture, thus increasing the resolution. If the desire is to constrain the array to the aperture spanned by the 63-sensor ULA and lower the sidelobe levels, then the solution is to use lower coprime factors.

Figure 2a shows an $M = 2$, $N = 3$ extended coprime array that matches the aperture of the 7, 9 design. In the basic 2, 3 design, subarray A has 2 sensors with $3d$ spacing and subarray B has 3 sensors with $2d$ spacing. The extended design concatenates multiple copies of this basic design to span the aperture of the 7, 9 coprime array.

Figure 4, a and **b**, compares the patterns for the unextended 7, 9 array and the extended 2, 3 design. Patterns are shown

on a log scale to better illuminate the sidelobes. Changing from the 7, 9 design to the 2, 3 design reduces the sidelobes of the multiplicative processor by 10 dB and those of the min processor by 23 dB. The cost for this improvement is additional sensors: the extended array has 39, whereas the unextended array has 15.

Further reduction in sidelobes is possible with adjustments of the weight vectors. A standard approach to lowering the sidelobes in a conventional beamformer is to apply a smooth taper that weights the outer sensors less than the center sensors (Van Trees, 2002). The cost of tapering is an increase in main lobe width. The weight vectors in **Figure 4, a** and **b**, use uniform tapers, which means that each sensor is weighted equally. **Figure 4c** shows the patterns for the 2, 3 design after a Dolph-Chebychev taper (Van Trees, 2002) has been applied. The resulting patterns have substantially lower sidelobes: −30 dB and −60 dB for the multiplicative and min processors, respectively. The tapered min processor with 39 sensors achieves essentially the same power pattern as the tapered ULA processor with 63 sensors.

Cross Terms Complicate the Picture

Based on the discussion in **Coprime Processing**, coprime multiplicative and min processors can achieve the same resolution as a ULA processor with fewer sensors. Extended arrays facilitate the design of processors with user-selected sidelobe levels. Equivalent performance with fewer sensors seems too good to be true. Are there other consequences of sparsity to worry about?

Figure 5 shows the output of the multiplicative and min processors for a planewave source at broadside plus spatially uncorrelated noise. The signal-to-noise ratio (SNR) at each sensor is 20 dB. The plots show the estimated power spectra obtained by scanning the directional cosines from −1 to +1. The narrowband input to the processors consists of a series of time snapshots. **Figure 5, a** and **b**, shows the average power spectra for the two processors as a function of the number of independent snapshots averaged. **Figure 5c** compares the final spectra from 10,000 snapshots with the ULA spectrum. The spectra for the multiplicative and min processors match the ULA spectrum for the source near broadside. The main differences between the coprime and ULA spectra are the signals that appear near $u = \pm 0.66$ and ±1. In the multiplicative spectrum, these false arrivals decrease with snapshot averaging. In the min spectrum, the false arrivals start low and do not decrease with averaging.

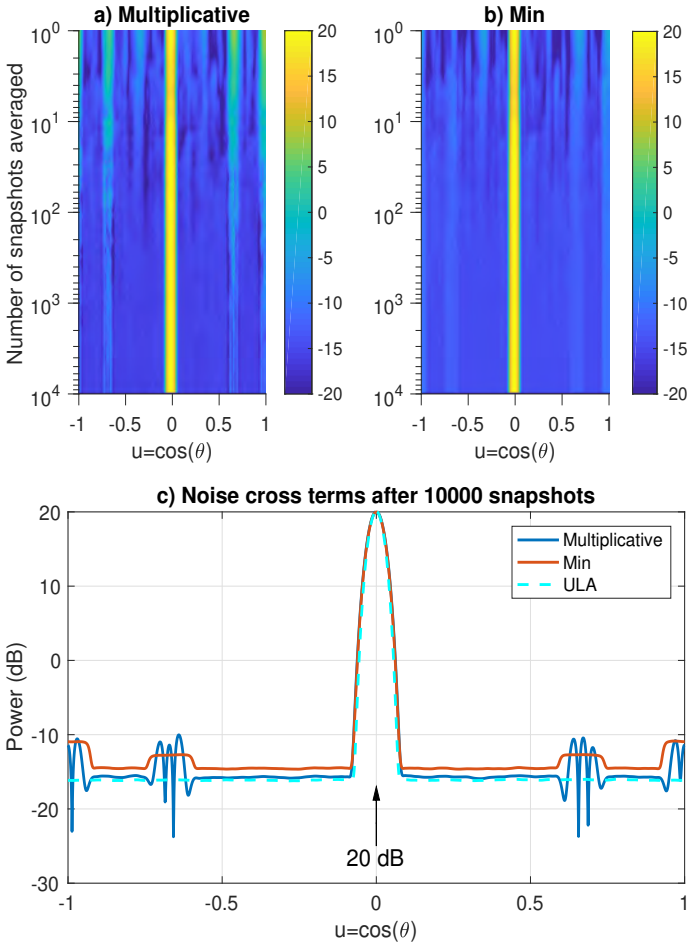

Figure 5. *Simulation illustrating source/noise cross terms for the* M *= 2,* N *= 3 extended coprime array with Dolph-Chebychev shading. Time-average spectra for the multiplicative (**a**) and min (**b**) processors are shown as a function of the number of scans averaged. **c**: Average spectra for the multiplicative, min, and ULA processors after 10,000 snapshots.*

The false arrivals are cross terms (Pedinoff and Ksienski, 1962), which arise when the input contains multiple sources. Cross terms form when a signal passing through subarray A interacts with a different signal passing through subarray B. When one or both of the signals in the cross term passes through a subarray grating lobe (rather than the main lobe), the cross term creates a false peak in the spectrum at a location away from either of the true signal directions. The source/noise cross terms shown in **Figure 5** occur when the loud planewave source aligns with one subarray's grating lobe and interacts with noise processed by the other subarray. This example shows that for high SNR sources, the min processor has substantially lower source/noise cross terms than the multiplicative processor. Averaging reduces the multiplicative cross terms when the sources are uncorrelated, although Chavali et al. (2014) found the decay to be slow: −5 dB per 10 snapshots. In **Figure 5**, it takes 10,000 snapshots for the multiplicative cross terms to reach the level of the min cross terms. Although the min processor is

less vulnerable to source/noise cross terms, an example in **Simulation Examples** shows that it is not immune to other types of cross term interference. Chavali (2017) and Liu and Buck (2018) provide detailed discussions of cross terms in multiplicative and min processors.

Simulation Examples

Figure 6 shows two simulations highlighting the competing strengths of the multiplicative and min processors. Both examples use the extended 2, 3 coprime design with Dolph-Chebychev weights. **Figure 6a** shows the simulation results for Case 1, which contains two high SNR sources near broadside and a low SNR (−5 dB) source at $u = -0.73$. Only 100 snapshots are available for averaging. The plot demonstrates that both the multiplicative and min processors resolve the sources near broadside with the same accuracy as the ULA. The main difference is that the min processor identifies the low SNR source, whereas the multiplicative processor does not because it is masked by the source/noise cross terms associated with the broadside sources. If 10,000 more snapshots were available, the multiplicative processor would reliably detect the low-level source.

Figure 6b shows the simulation results for Case 2, which has sources at $u = -0.5$, 0.66, and 1 with SNRs of 0, 8, and 16 dB, respectively, and 10,000 snapshots available for averaging. In this scenario, the multiplicative processor outperforms the min processor. The plot shows that the min processor has large peaks at $u = -0.33$ and 0, in addition to the peaks at the source locations. These false peaks are cross terms due to the loud sources at $u = 0.66$ and 1. To see how the cross term at $u = 0$ is generated, consider the beampatterns in **Figure 4c**. When the array is steered to broadside, the subarray grating lobes align with the sources at $u = 0.66$ and 1. Thus, the min processor sees large signals coming through both subarrays simultaneously, and the result is a peak in the spectrum. The cross terms in the multiplicative processor occur at the same locations, but they are reduced through averaging (because the sources are uncorrelated).

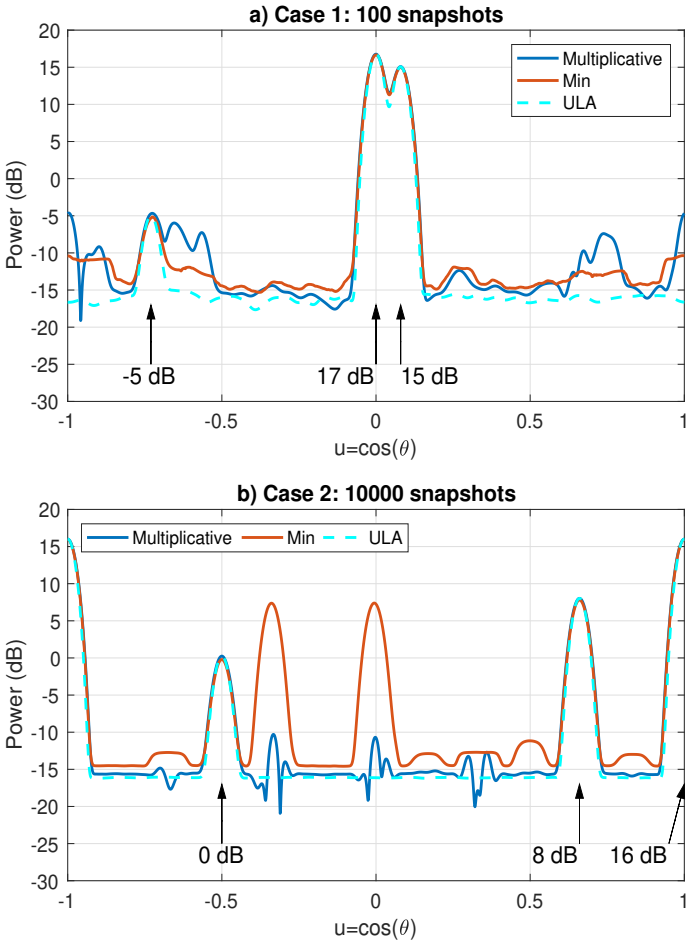

Figure 6. *Simulation examples for two cases utilizing the extended Dolph-Chebychev-shaded coprime array.* ***a****: Case 1 illustrates how a cross term generated by loud sources near broadside masks a low-level source in the multiplicative power estimate. The min processor detects the quiet source in this case.* ***b****: Case 2 demonstrates that snapshot-averaging mitigates cross terms, resulting in an accurate multiplicative spectrum, whereas the min spectrum contains large false peaks.*

Conclusion and Suggestions for Further Reading

This article showed how to use aliased subarrays to achieve the same resolution as a ULA with fewer sensors. Multiplicative and min processors eliminate ambiguities due to undersampling, and weights can be designed to control sidelobe levels to facilitate detection of low-level sources. In some environments, cross terms can mask sources or generate false detections, but time averaging or processor selection (switching between min and multiplicative depending on spatial distribution of sources and relative SNRs) can mitigate their effects. When sensors are expensive, sparse arrays and processing algorithms are a viable cost-saving alternative to densely spaced uniform arrays.

Here are a few suggestions for further reading on this subject. Although this article focused on coprime arrays, the same processing approaches are applicable to nested geometries. Chavali (2017) compares the performance of the multiplicative and min processors for coprime and nested arrays using experimental data from a challenging underwater acoustic environment. The examples in this article use passive (receive-only) arrays, but similar processing approaches have been applied to active (transmit/receive) arrays. Hoctor and Kassam (1990) discuss both active and passive applications, and Mitra et al. (2010) describe using polynomial factoriza-

tion to design patterns for active ultrasound arrays. Because the power spectrum and the spatial covariance are related through a Fourier transform, multiplicative and min processing can estimate a spatial covariance function (Adhikari and Buck, 2017; Liu and Buck, 2017).

Pillai and Haber (1987) describe an intriguing technique for synthesizing an augmented covariance matrix from an estimated covariance function derived from a single sparse array. Their approach facilitates high-resolution localization of *more sources than sensors*. Vaidyanathan and Pal (2011) and Liu and Buck (2016, 2017) extend the augmented covariance approach from a single array to the interleaved sparse arrays discussed in this article.

The articles described above represent a small sample of the current research. For more of the latest results, see the special issue of *The Journal of the Acoustical Society of America* (June 2018) on compressive sensing in acoustics (acousticstoday.org/compressive-sensing), which has four articles on coprime array processing along with related articles on the topic of direction-of-arrival (DOA) estimation using sparsity constraints (Gerstoft et al., 2018).

Acknowledgments

This work was supported by Office of Naval Research (ONR) Awards N0000014-13-1-0229 and N00014-17-2734. Kathleen E. Wage thanks Professor John R. Buck and Mr. Vaibhav Chavali for many useful discussions and the University of Rhode Island Ocean Engineering Department for hosting her recent sabbatical.

References

Adhikari, K., and Buck, J. R. (2017). Spatial spectral estimation with product processing of a pair of colinear arrays. *IEEE Transactions on Signal Processing* 65, 2389-2401. https://doi.org/10.1109/TSP.2017.2659642.

Adhikari, K., Buck, J. R., and Wage, K. E. (2014). Extending coprime sensor arrays to achieve the peak side lobe height of a full uniform linear array. *EURASIP Journal on Advances in Signal Processing* 201, 1-17. https://doi.org/10.1186/1687-6180-2014-148.

Berman, A., and Clay, C. S. (1957). Theory of time-averaged-product arrays. *The Journal of the Acoustical Society of America* 2, 805-812. https://doi.org/10.1121/1.1909060.

Chavali, V. (2017). *Coprime and Nested Processing of the Elba Island Sonar Data Set*. MS Thesis, George Mason University, Fairfax, VA. https://doi.org/10.13021/G8JX0W.

Chavali, V., Wage, K. E., and Buck, J. R. (2014). Coprime processing for the Elba island sonar data set. *2014 48th Asilomar Conference on Signals, Systems, and Computers*, Pacific Grove, CA, November 2-5, 2014, pp. 1864-1868. https://doi.org/10.1109/ACSSC.2014.7094791.

Davies, D. E. N., and Ward, C. R. (1980). Low sidelobe patterns from thinned arrays using multiplicative processing. *IEE Proceedings F (Communications, Radar, and Signal Processing)* 127, 9-15. https://doi.org/10.1049/ip-f-1.1980.0002.

Di Martino, G., and Iodice, A. (2015). Coprime synthetic aperture radar (CopSAR): A new acquisition mode for maritime surveillance. *IEEE Transactions on Geoscience and Remote Sensing* 53(6), 3110-3123. https://doi.org/10.1109/TGRS.2014.2369035.

Gerstoft, P., Mecklenbräuker, C. F., Seong, W., and Bianco, M. (2018). Introduction to compressive sensing in acoustics. *The Journal of the Acoustical Society of America*, 143(6), 3731-3736. https://doi.org/10.1121/1.5043089.

Hoctor, R. T., and Kassam, S. A. (1990). The unifying role of the coarray in aperture synthesis for incoherent and coherent imaging. *Proceedings of the IEEE* 7, 735-752. https://doi.org/10.1109/5.54811.

Johnson, D. H., and Dudgeon, D. E. (1993). *Array Signal Processing*. Prentice Hall, Englewood Cliffs, NJ.

Liu, Y., and Buck, J. R. (2015). Detecting Gaussian signals in the presence of interferers using the coprime sensor arrays with the min processor. *2015 49th Asilomar Conference on Signals, Systems, and Computers*, Pacific Grove, CA, November 8-11, 2015, pp. 370-374. https://doi.org/10.1109/ACSSC.2015.7421150.

Liu, Y., and Buck J. R. (2016). Super-resolution DOA estimation using a coprime sensor array with the min processor. *2016 50th Asilomar Conference on Signals, Systems, and Computers*, Pacific Grove, CA, November 6-9, 2016, pp. 944-948. https://doi.org/10.1109/ACSSC.2016.7869188.

Liu, Y., and Buck, J. R. (2017). High-resolution direction-of-arrival estimation in SNR and snapshot challenged scenarios using multi-frequency coprime arrays. *2017 IEEE International Conference on Acoustics, Speech, and Signal Processing (ICASSP)*, New Orleans, LA, March 5-9, 2017, pp. 3434-3438. https://doi.org/10.1109/ICASSP.2017.7952794.

Liu, Y., and Buck, J. R. (2018). Gaussian source detection and spatial spectral estimation using a coprime sensor array with the min processor. *IEEE Transactions on Signal Processing* 66(1), 186-199. https://doi.org/10.1109/TSP.2017.2762284.

Mitra, S. K., Mondal, K., Tchobanon, M. K., and Dolecek, G. J. (2010). General polynomial factorization-based design of sparse periodic linear arrays. *IEEE Transactions on Ultrasonics, Ferroelectrics, and Frequency Control* 57, 1952-1966. https://doi.org/10.1109/TUFFC.2010.1643.

Pal, P., and Vaidyanathan, P. P. (2010), Nested arrays: A novel approach to array processing with enhanced degrees of freedom. *IEEE Transactions on Signal Processing* 58(8), 4167-4181. https://doi.org/10.1109/TSP.2010.2049264.

Pedinoff, M., and Ksienski, A. (1962). Multiple target response of data-processing antennas. *IRE Transactions on Antennas and Propagation* 10, 112-126. https://doi.org/10.1109/TAP.1962.1137837.

Pillai, S. U., and Haber, F. (1987). Statistical analysis of a high resolution spatial spectrum estimator utilizing an augmented covariance matrix. *IEEE Transactions on Acoustics, Speech, and Signal Processing* 35, 1517-1523. https://doi.org/10.1109/TASSP.1987.1165068.

Ryle, M. (1952). A new radio interferometer and its application to the observation of weak radio stars. *Proceedings of the Royal Society of London A: Mathematical, Physical and Engineering Sciences* 211, 351-375. https://doi,org/10.1098/rspa.1952.0047.

Shaw, E., and Davies, D. E. N. (1964). Theoretical and experimental studies of the resolution performance of multiplicative and additive aerial arrays. *Radio and Electronic Engineer* 28, 317-324. https://doi.org/10.1049/ree.1964.0136.

Vaidyanathan, P. P., and Pal, P. (2011). Sparse sensing with co-prime samplers and arrays. *IEEE Transactions on Signal Processing* 59, 573-586. https://doi.org/10.1109/ACSSC.2010.5757766.

Van Trees, H. L. (2002). *Optimum Array Processing*. John Wiley & Sons, Inc., New York.

Welsby, V. G. (1961). Multiplicative receiving arrays: The angular resolution of targets in a sonar system with electronic scanning. *Journal of the British Institution of Radio Engineers* 22, 5-12. https://doi.org/10.1049/jbire.1961.0077.

BioSketch

Kathleen E. Wage is a signal processor whose current interests are sparse arrays, random matrix theory, underwater acoustics, and engineering education. She is an associate professor of electrical and computer engineering at George Mason University, Fairfax, VA. Kathleen obtained her BS

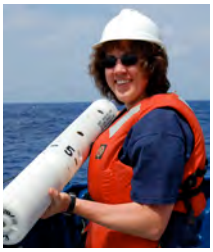

in electrical engineering from the University of Tennessee, Knoxville, and her MS and PhD in electrical engineering from the MIT/Woods Hole Oceanographic Institution Joint Program. She received the 2016 IEEE Education Society/Hewlett-Packard Harriett B. Rigas Award. Kathleen spent 55 days at sea for the PhilSea experiments and wishes the Olympic Committee would recognize "Sonobuoy Tossing" as an official sport.

NEWS *from the* Acoustical Society Foundation Fund

This is my first column as chair of the Acoustical Society Foundation, and I want to thank Carl Rosenberg for his many years of service as chair of the Board. Fortunately, he has agreed to stay on the Board, and we look forward to working together to help the Society.

One of the purposes of this column is to recognize the various ways that members help the Society. Acoustical Society of America (ASA) Fellow Jerry Hyde has notified the Foundation that he and his wife Michele have established a living trust through the Foundation Fund. This gift will support significant scholarships for study in architectural acoustics and noise control (Jerry's fields). Jerry writes, "My life and career have benefited from my association with the ASA. I started as a lab assistant for Vern Knudsen as a young physics student at the University of California, Los Angeles (Izzy Rudnick was my faculty advisor), and my career in acoustics blossomed from there. The main thing is to leave a lasting legacy that reflects my appreciation for the values of the Society that I've now been a member of for over 50 years." Jerry also hopes this gift will be an inspiration for others to do the same. With a living trust, the donors maintain the earnings of the donation until the trust is terminated, and the ASA receives the benefit of the donation in the future. I would like to express our appreciation for Jerry and Michele's generosity. The Foundation welcomes and greatly values gifts of all sizes, and some of these will be highlighted in future columns.

James H. Miller
Chair, Acoustical Society Foundation Board
miller@uri.edu

Mission of the Acoustical Society Foundation Board:
To support the mission of the ASA by developing financial resources for strategic initiatives and special purposes.

ASFF *For more information, contact James H. Miller at miller@uri.edu*